Time Dependent Surface Corrosion Analysis and Modelling of Automotive Steel under a Simplistic Model of variations in Environmental Parameters

Dr. Adil Saeed (corresponding author)

NanoCorr, Energy & Modelling Research Group
Faculty of Science and Technology
Bournemouth University Talbot Campus, Poole, Dorset BH12 5BB
Tel: 0044-1202-965732
Email: asaeed@bournemouth.ac.uk

Dr. Zulfiqar A Khan

NanoCorr, Energy & Modelling Research Group
Faculty of Science and Technology
Bournemouth University Talbot Campus, Poole, Dorset BH12 5BB
Tel: 0044-1202-961645
Email: zkhan@bournemouth.ac.uk

Dr Mian Hammad Nazir

NanoCorr, Energy & Modelling Research Group
Faculty of Science and Technology
Bournemouth University Talbot Campus, Poole, Dorset BH12 5BB
Email: hnazir@bournemouth.ac.uk

Abstract

This research presents time-dependent corrosion analysis of automotive steel utilised in a large military vehicle in real operating environment, followed by simulated environmental tests and simplistic surface corrosion modelling. Time-dependent surface corrosion accumulated on this specific component was observed to be approximately 250 µm thick, with the identification of surface contaminants such as chlorine and sulphur. Simulated environmental tests considering temperature and relative humidity variations were performed to evaluate quantitative corrosion damage to the structure of the vehicle. The relationship of various temperatures and relative humidity with respect to time, within the context of corrosion initiation and propagation, has been presented. A mathematical model to incorporate corrosion accumulation on the surfaces derived from the simulated environmental tests is presented.

Keywords: Oxidation, Environmental, Simulation, Structural Failures, Metal-scale

Nomenclature

$i(t)$	Corrosion current density
$i_1(t), i_2(t), i_3(t)$	Current densities in phases 1-3 respectively
$c(t)$	Instantaneous corrosion rate
$C(O_2)$	Oxygen concentration in environment directly related to RH
dm/dt	Metal loss rate
$m(t)$	Actual metal loss
n	Number of electrons in the oxidation process
D	Diffusivity of oxygen through water vapour
δ	Thickness in water vapour (concentration gradient)
t_a	Time scale value for point of interface of phase 1 and 2
t_m	Time scale value for point of interface of phase 2 and 3
t_f	The final time at which the metal loss process ceases.
t_L	Process time spent during phase 3
$C_B(O_2)$	Bulk oxygen concentration in water vapour
$D_B(T)$	Diffusivity of Bulk oxygen concentration
$C_R(O_2)$	Effective oxygen concentration needed to drive Oxygen
$C_m(O_2)$	Minimum Oxygen concentration below rust
$R(t)$	Thickness of corrosion product
P	Metal loss per unit concentration gradient
S_1, S_2, S_3, S_4, S_5	Terms derived from metal loss equation with S_1, S_2, S_4 being variables and S_3, S_5 as constant.
m_m and m_f	Initial and final metal loss values respectively

1   Introduction

Large military vehicles operate in parts of the world that are linked to various types of structural failures influenced by corrosion, which is a time-dependent phenomenon. The location could be from aggressive marine environment with salt spray to desert with wind full of sand particles and stern temperatures; such dynamics of changing temperatures and severe operating conditions are closely related to component failures. After 18 years of service 25% of the Canadian Army fleet suffered noticeable structural corrosive failures [1, 2]. Costs of corrosion maintenance are high and approximately 40% of the US defence budget is spent on corrosion related failures [2]. Vehicles which were exposed to such environments and operating conditions undergo structural degradation when stored stationary for an unidentified period in shelters or open spaces.

This research reports corrosion failure analysis and mathematical modelling for the sample collected from a large military vehicle used as Military Tank Destroyer; that displays corrosion in its structure in various modes and has pronounced effects on its structural integrity.

This vehicle was designed and manufactured in the US, and was initially used as a dedicated military tank destroyer and to lead the armour combat. A large number of this type of vehicles were acquired by the British Army, and modified according to their needs. It served in anti-tank regiments of the Royal Artillery. One of these types of vehicle is now stationed in a sheltered facility. This vehicle is undergoing structural failures because of corrosion problems which have been stockpiled during/after its service life.

The correlation between environment and corrosion on this large vehicle was investigated for the purpose of its life expectancy. This is the first kind of fundamental study conducted to investigate corrosion damage within these vehicles. Based on the experimental data gathered, a mathematical model based on a simplistic model of variations in temperatures and relative humidity is designed to explain the mechanisms behind the surface corrosion propagation under controlled environment. This research paper is a part of the wider project focusing on the materials degradation through corrosion and failure predictions in large vehicles [3-16].

2   Experimental Methodology

A sample with dimensions 102 mm x 94 mm was collected from the inside armour of this vehicle. This sample was corroded on one side while the other side had some protection in the form of previously applied coating. The current research reported in this paper has been conducted in 4 distinct stages 1): Materials characterisation was conducted to obtain the materials composition 2) Investigation of existing surface corrosion and sub-surface defects 3): Accelerated simulated environmental tests (aSET) and 4): Mathematical modelling of surface corrosion derived from the aSET.

2.1   Materials Characterisation

The materials composition of the sample was unknown. For this purpose one side (edge) of the sample was cross sectioned to achieve a nascent surface free from surface deposits and contaminants. On this newly exposed surface x-ray fluorescence technique (XRF) was conducted to achieve the sample materials composition provided in Table 1.

Table: 1 Material Composition of the Sample [17]

Constituents	Si	P	Cr	Mn	Ni	Cu	Mo	Fe
Percentage	0.13	0.02	0.06	0.4	0.03	0.09	0.05	Remainder

2.2 Sample Conditioning for Surface and Sub-surface Corrosion Analyses

Corrosion was analysed on the sample in the following sequence:

a) Existing surface corrosion was analysed on the corroding surface to obtain corrosion morphology and to characterise corrosion products.
b) To evaluate corrosion propagation/corrosion layer-depth and to investigate sub-surface defects, sample was sectioned and mounted in Bakelite.

2.3 Samples Preparation for Accelerated Simulated Environmental Tests

Sample collected, was sectioned for these tests. Four samples with dimension of 4 cm long and 3 cm wide were prepared. These samples were previously corroded, thus corrosion from the surfaces was effectively removed using Silicon Carbide papers of varying grades. These samples were polished to achieve average surface roughness of less than 1 μm, rinsed with de-ionised water and dried immediately. No chemicals were used during this samples preparation process.

2.3.1 Tests Conditions

Experimental conditions were defined for the simulated environments tests to include relative humidity (RH) and temperatures (T) presented in Table 2. This model takes into consideration the comfort level of the personnel and avoids wet-dry cycles [18]. Each sample was exposed separately to the selected T and RH for 125 hours. In the first part of the test, temperature of the chamber was kept constant at 18 degree Celsius and two values of RH 35% and 55% were used for 125 hours each. In second part of the environmental test, RH was kept constant at 40% and two temperatures 5 and 25 degree Celsius were used for 125 hours.

Table: 2 Accelerated Environmental Tests Conditions and % age of Accumulated Corrosion [17].

Wolverine - M10 Tank destroyer						
Sample No	Temperature (°C)	Relative Humidity (%)	Exposure Time (Hours)	Sample Area (mm²)	Corrosion Area (mm²)	Corrosion %
1	5	40	125	542.69	2.95	0.54
2	25	40	125	527.05	1.07	0.20
3	18	35	125	519.14	0.14	0.03
4	18	55	125	533.99	5.40	1.01

2.3.2 Corrosion Area Quantification

Corrosion was accumulated on all four samples after exposure to aSET. Complex morphology was observed in the accumulated corrosion. To quantify corrosion build up; first, high definition images of the samples were taken using state-of-the-art macro imaging tools; secondly, quantification of the corrosion build-up was performed through image analysis software.

2.4 Mathematical Modelling

A simplistic model incorporating Temperature and Relative Humidity presented based upon aSET's results. This model is deployable for the vehicles which are kept inside the sheltered facility assuming failures progressing through coatings without considering environmental pollutants.

3 Results and Discussion

3.1 Shelter's inside Environment

Though it is not advisable to keep the temperatures below/above the comfort level of the personnel, however variations in T and RH result in atmospheric corrosion in the vehicles.

The internal environment of the shelter is steady where natural daylight together with fluorescent tubes is used for lighting purposes. Temperatures are controlled during winter but not in summer whereas humidity is not controlled in any season. In winter temperature is kept between 18 and 25 degree Celsius, humidity in this shelter during the months of October - December and January - March often reaches 75 - 80%, however, an increase to 95 - 100% has been also recorded on several occasions. Temperatures fluctuations during the same months were recorded between 5 and 20 degree Celsius. Readings obtained from the Temperature - RH sensors installed in the open turret of this vehicle have shown, RH reaching as high as 80% during October - December. During the period of January - March RH has been observed to reach nearly 70%. Temperature for both durations was not steady and fluctuated between minimum 13 and maximum 23 degree Celsius. During these periods formation of condensation/moisture has been observed on the tank surfaces.

3.2 Existing Surface and Sub-surface Analyses

Figure 1 shows Scanning Electron Micrograph (SEM) of the corroding surface, three spectra 1, 2 and 3 were measured and results are given in Table 3. All three spectra exhibit similar oxidation of 42wt%. In spectrum 2 chlorine (1.47 wt%) was detected, whereas Iron (Fe) was recorded at the lowest (52.66wt%) at spectrum 3.
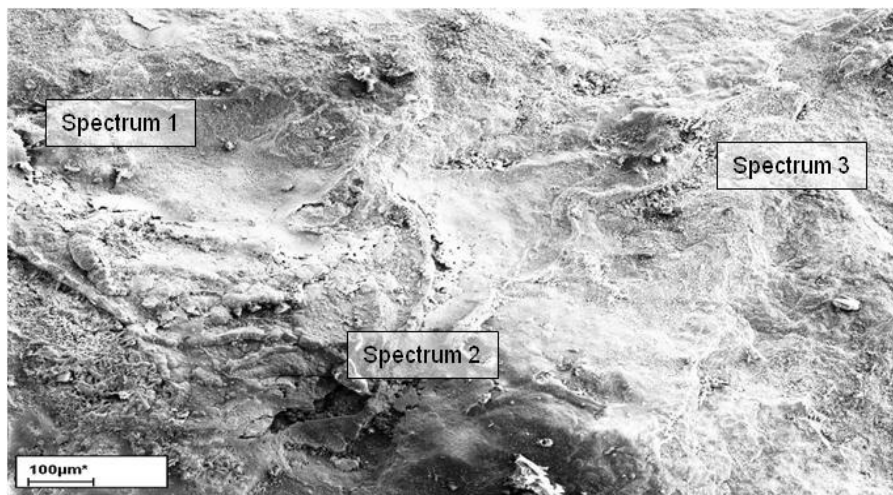

Figure 1 SEM Micrograph showing EDS spectra location at corroding surface [17].

Table: 3 Spectra Results at the Corroding Surface [17].

Wolverine - M10 Tank Destroyer Corroding Surface (results in weight %)					
Elements normalised					
Spectrum	O	Al	Si	Cl	Fe
1	41.50	2.43	1.54	0.00	54.53
2	42.15	1.68	1.02	1.47	53.67
3	42.98	2.33	1.43	0.59	52.66

Cross section of the sample was examined that showed sub-surface corrosion propagation to a depth of 250 µm shown in Figure 2(a). This analysis identified defects such as slags shown in Figure 2 (b) and (c). Results of two Energy Dispersive Spectroscopy (EDS) spectra 1 in the slag & 2 near the slag, [Figure 2(c)] are given in Table 4. Spectrum 1 showed sulphur (S) together with silicon (Si), oxygen (O) and Fe only 68.22wt%. Spectrum 2 however showed Fe (98.98wt%) with only manganese (Mn). In the cross section at the bulk metal where no corrosion has reached, six spectra were measured shown in Figure 2(d). Results showed Fe above 99wt% with only Mn less than 0.50wt%.
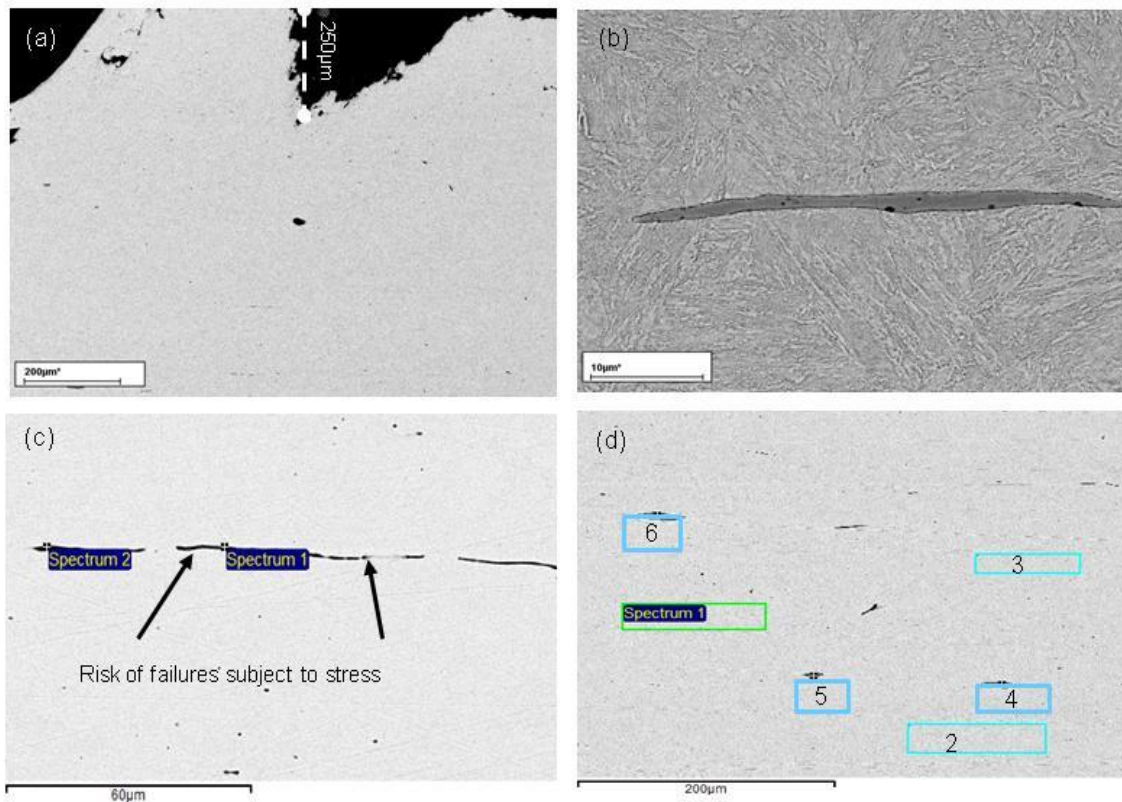

Figure: 2 (a) Corrosion propagation (b) SEM (back scattered) micrograph of slag 1 inclusion (c) SEM (secondary electron) micrograph of slag 2 inclusion (d) Six spectra at bulk metal rectangles represent EDS areas [17].

Table: 4 Slag Inclusion Results in the Cross Section [17].

Wolverine- M 10 Tank Destroyer Slag Inclusion (results in weight %)					
Elements normalised					
Spectrum	O	Si	S	Mn	Fe
1	7.32	2.13	4.76	17.57	68.22
2	0.00	0.00	0.00	1.02	98.98

Atmospheric corrosion is hugely influenced by RH, temperature and pollutants. During conditions when temperature is greater than 0 degree Celsius and RH ≥ 80%, build-up of condensation or thin water film on the surfaces will result in Time of Wetness (TOW) and consequently atmospheric corrosion [19]. In addition this vehicle is sheltered with no/negligible washing effect causing extended TOW and periods of dew [19, 20]. When RH > 80%, rust layer on the surfaces becomes hygroscopic particularly on Fe, Cu, Zn and Ni and they corrode preferentially. In winter, during nights heating in the sheltered facility is switched off/or lowered down and starts to function in the morning. This rise in ambient temperature in the morning compare to the vehicle surfaces which are at lower temperatures may deliver dew point condensation, therefore rapid corrosion is expected due to fast electrochemical reaction and diffusion rate which could increase with rising temperature [20].

Internal environment of this sheltered facility can be considered free from atmospheric pollutants; however corrosion initiating contaminants such as Cl and S were detected on the vehicle's surfaces (Table 3 & 4). Conductivity of the electrolyte is also a major factor in determining the rate of corrosion, which is dependent on the level of dissolved contaminants. The Sheltered facility for the large vehicles is in Bovington United Kingdom, which is approximately 9 km away from the English Channel/sea. Sea winds are source of aerosols particles. Sea salt consists approximately 55% Cl^-, 30% Na^+, 8% SO_4^{-2} and 1% Ca^{+2} by weight. It has been reported that salt particles (aerosols) in approximate sizes of (12 - 40 μm) could be deposited on the structures which are located up to 10 km from the coastline [21]. Spray due to sea winds result in chloride deposition in the form of droplets or crystalline form on surfaces. Coal burning incinerators de-icers, bleaching plants and dust-binders on roads may also emit chlorides. Corrosion of metals can occur at low humidity such as 35% in the presence of chlorides. Steel corrodes at higher rate when exposed to continuous spray of salt. Figure 3 illustrates formation of the typical oxide-layer on a metal surface which consists of pores and cracks. Through these pores and cracks chlorine can reach the substrate and may provide fast diffusion paths, thus resulting in metal chlorides and escalated corrosion. Oxygen potential is very low at the metal-scale interface because oxygen (O_2) produces metal oxides, its consumption is more and the diffusion of gases through metal-scale interface will determine the corrosion rate [20, 22-24].
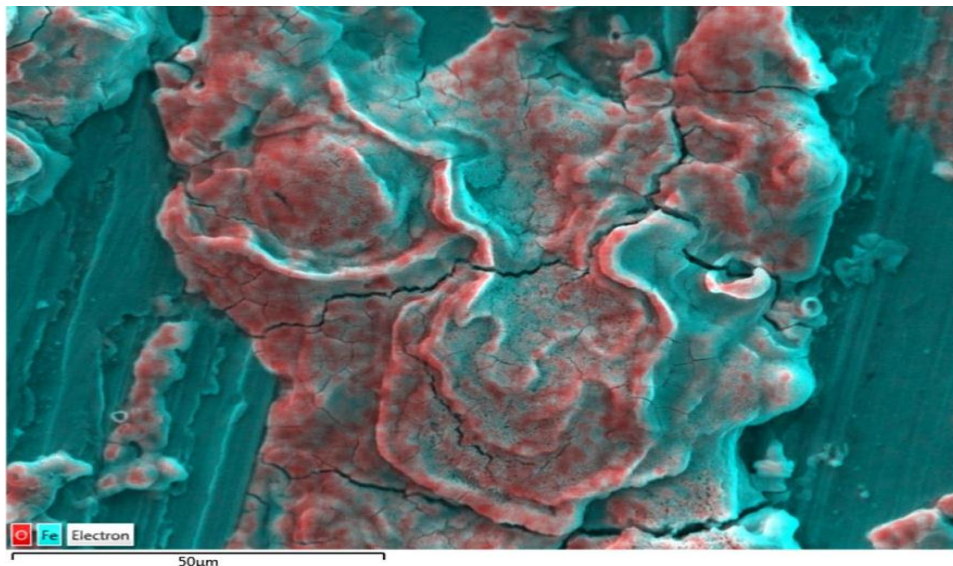

Figure: 3 Formation of Corrosion Layer on sample 4 illustrating Fe and O [17].

A large military vehicle has a complex geometrical configuration and is comprised of several components where dirt, moisture and other atmospheric contaminants can easily be deposited. The accumulation of Cl is also expected in many crevices of this vehicle and Cl

influenced localised corrosion is likely in many parts of its structure. Aluminium (Al) was also recorded on the corroding surface (Table 3). However, during analysis at the cross section (Figure 2d), no Al was identified. Presences of the Al at three spectra on the corroding surface could be classified as residues from Al based paints as protection applied during/after vehicle's service life.

Slag (Figure 2 b-c) is a by-product of metal oxide and silica (SiO_2) and tend to promote crack propagation starting from the slag-vein and could result fatigue failures under stress in operating conditions which could be assumed safe for the working components [25]. Such defects are not favourable in heavy duty mechanical structures. The detection of S at spectrum 1 Figure 2 (c), Table 4, in the vicinity of the grain boundaries can compromise physical as well as structural properties of the materials [26, 27]. This type of defect will usually give rise to Mode I fracture failure, the opening crack propagation mode, when subjected to tensile loading. When the stress intensity factor (K), also known as material fracture toughness, reaches a critical value, crack propagation will take place. The stress intensity factor (K) is used in fracture mechanics to predict "Stress intensity" or the state of the stress near the crack tip resulted as a consequence of residual stress or load. It depends on the type of materials, materials processing, rate of loading, state of stress and temperatures. Such material inherit defects affect this value, hence making component susceptible to mechanical failures when subjected to loading. S arises from the steel making process and to avoid the formation of FeS, Mn is added to steel to form MnS which is thermodynamically stable. However MnS exposed to (Cl^-) may initiate pitting corrosion [28-32].

3.3   Accelerated Simulated Environmental Tests (aSET)

The purpose of aSET was to extrapolate the results for the purpose of corrosion behaviour when large vehicles are kept in a controlled environment considering visitors comfort. aSET were conducted taking into account only temperature and RH. Parameters such as pH, corrosive deposits on the surfaces and nature of the electrolyte are not considered in this paper. Exposure to simulated environmental corrosion tests illustrated build-up of surface corrosion with complicated shapes and morphology on all the samples. Sample 4, which was exposed to18 degree Celsius and 55% RH showed the highest percentage of corrosion. Table 2 provides the total percentage of the accumulated corrosion on each sample. Figure 4 illustrates the concentration of Fe and O at sample 4 after exposure to aSET.
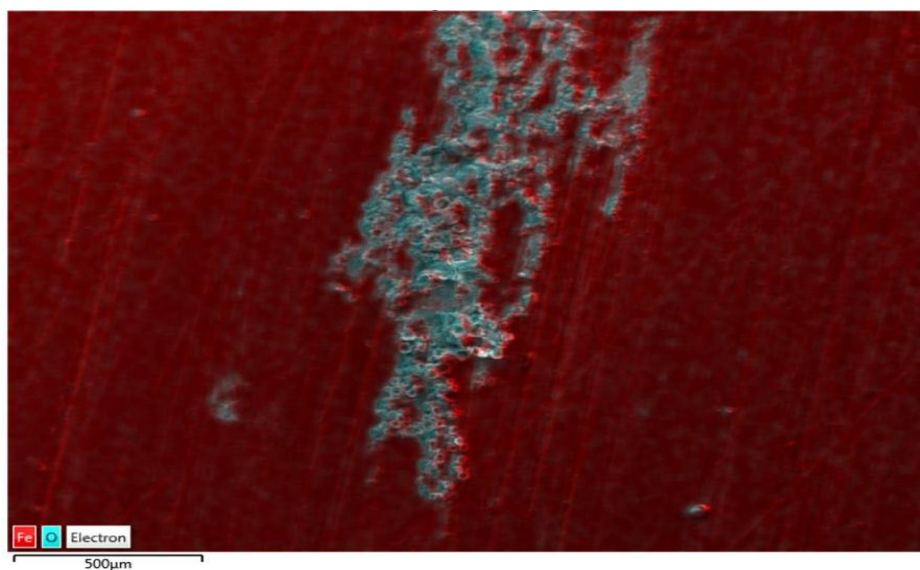

Figure: 4 Sample 4 (18 degree Celsius - 55 % RH) illustrating concentrations of Fe and O [17]

Results in Table 2 identify the importance of RH control. When temperature is maintained between 5 and 25 degree Celsius with a constant 40% RH, the corrosion rate is less than 1%. However increase in RH to 55% increases corrosion rate to almost double. The control of RH is an important factor for this sheltered facility for large vehicles to diminish corrosion. Areas, where the control of humidity is not possible, a lower temperature may be suitable to reduce the TOW and consequently corrosion rate [33]. Increase in temperature cause fast diffusion-rate and corrosion, but increase in temperature under constant humidity evaporates the electrolytic-layer created through dew/rain and produces dry-conditions [20, 34]. Results of sample 4 could be attributed to such conditions where temperatures was not high enough to evaporate the electrolytic-layer and provided extended time-of-wetness for the electrochemical process to continue. Conversely in the case of other samples dry atmospheres may have been achieved and hence corrosion rate was slow. Carbon steel is not able to form a protective layer against corrosion except when the atmosphere is clean and dry [35].

The surfaces of this large vehicle are contaminated and humidity reaches above 80% in some cases. This will result corrosive electrolytic layer on the surfaces because of hygroscopic salts, accordingly rapid corrosion may occur in the vehicle components and on the surfaces. Also the role of oxygen is important here as an oxidant element in the atmospheric corrosion, the water layer formed on the metallic surfaces determine oxygen diffusion towards the surfaces and reaction products [20, 36].

Figure 3 of sample 4 illustrates the build-up of a typical oxide layer on steel and reflects the characteristics of lepidocrocite (γ-FeOOH) and goethite (γ- Fe_2O_3) of rust layer for a non-polluted environment. These layers have various types of cracks, pores, poor adherence and flake away from the surfaces depending on localised corrosion; this type of rust layer cannot result as a passivation and therefore electrolyte and corrosive contaminants can reach the steel substrate [24, 34, 37].

3.4 Multiple Phase Model: Corrosion Condition Monitoring for Controlled Environmental Conditions

On the basis of data from aSET Figure 5, a multiple phase corrosion condition monitoring model (ACCM) is proposed. The propose model takes into consideration the variation of RH along the metal interface. The mathematical model is divided in to three main phases shown in Table 5 and mathematical description for all the phases and their interrelationship is presented in next section.
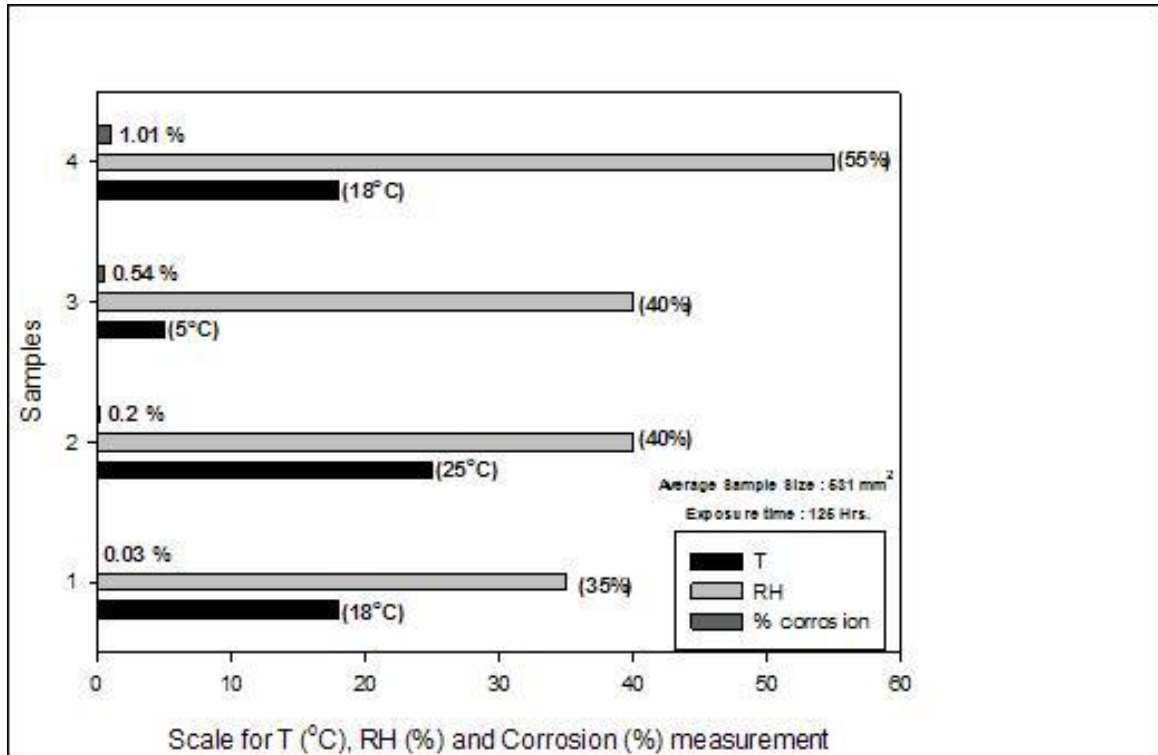
Figure 5 M-10 Environmental condition and % Corrosion formation

Table 5 Phases of ACCM and Description

Phase No	Description of ACCM phases	Current densities
1	A very short term phase including the oxygen concentration to build up to the required level to activate the process of corrosion	$i_1(t)$
2	Includes the Oxygen diffusion through water vapour layer towards iron	$i_2(t)$
3	Includes the Oxygen diffusion through corrosion product formed at bare iron	$i_3(t)$

3.4.1 Mathematical Design for Multiple Phase Atmospheric Corrosion Condition Monitoring (ACCM)

Experimental results of aSET justify that RH has a vital role in corrosion initiation and progression. Corrosion mechanics for the aSET experimental work can be described by a simplified theory shown in Figure 6.
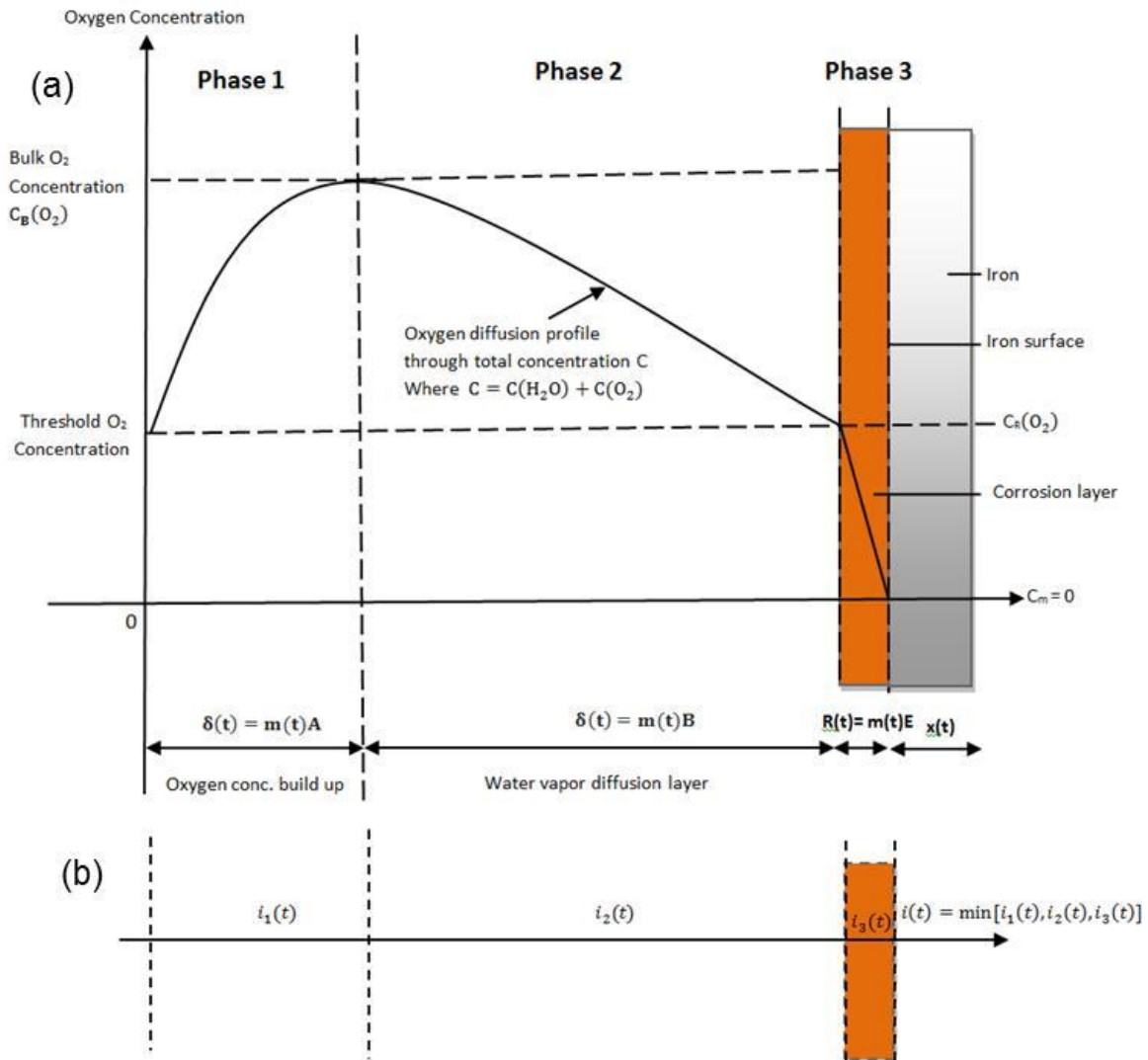
Figure: 6 (a) Oxygen concentration profile (i) water vapour + O_2 - phase 2 and (ii) Corrosion Product - phase 3, (b) Corrosion current density through water vapour and rust layer

It is well known that,

$$RH = (\rho_w / \rho_{ws}) * 100 \qquad\qquad 1$$

ρ_w is the vapour partial pressure and ρ_{ws} is the saturation vapour partial pressure of water vapour given as $\rho_{ws} = 6.1 * 10^{\frac{7.5*T}{237.3+T}}$. ρ_{ws} rise with increase in temperature T. The amount of water vapours in air increases with increase in dew point temperature T_d, which is given as $\rho_w = 6.1 * 10^{\frac{7.5*T_d}{237.3+T_d}}$. Thus, ρ_w rises with the increase in T_d resulting in higher concentration of water vapour in air. Water vapour concentration (Kg/m^3) found in air is,

$$C(H_2O) = 0.00216 * \left(\frac{\rho_w}{273.15+T} \right) \qquad\qquad 2$$

It is assumed that the vapour partial pressure in air do not take into account any non-volatile solute e.g. pollutants. Non-volatile solutes can change the vapour partial pressure of pure water in air. Let $C(O_2)$ be the concentration of Oxygen in the air. The diffusion of Oxygen in air will depend on $C(H_2O)$. Considering the negligible effect of other atmospheric gases on the diffusion of Oxygen, the total concentration can be written as,

$$C = C(H_2O) + C(O_2) \qquad\qquad 3$$

Flux of Oxygen (N_{O2}) through water vapour is made up of two components, namely that result from the bulk motion ($x_O N_B$) and that from molecular diffusion J_O,

$$N_{O2} = x_O\, N_B + J_O \qquad\qquad 4$$

$J_O = -D_{(H_2O),O_2}(T)\frac{C(O_2)}{\delta}$ but for simplicity we consider, $D_{(H_2O),O_2}(T) = D(T)$ and therefore substituting it in eq. 4 gives,

$$N_{O_2} = x_O N_B - D(T)\frac{C(O_2)}{\delta} \qquad\qquad 5$$

As $N_B = N_{O_2} + N_{H_2O}$ and $x_O = \frac{C(O_2)}{C}$, eq. 5 becomes,

$$N_{O_2} = \frac{C(O_2)}{C}(N_{O_2} + N_{H_2O}) - D(T)\frac{C(O_2)}{\delta} \qquad\qquad 6$$

Rearranging terms and integrating between the plane, (higher Oxygen concentration) and plane 2 (lower Oxygen concentration).

$$\int \frac{\delta}{CD(T)} = \int_{C(O_2)_1}^{C(O_2)_2} \frac{C(O_2)}{N_O C - C(O_2)(N_{O_2} + N_{H_2O})} \qquad\qquad 7$$

As water vapour is a non- diffusing element therefore, $N_{H_2O} = 0$. Also total concentration C is assumed to remain constant. Eq. 7 can be written as,

$$N_{O_2} = \frac{D(T)C}{\delta}\ln\left(\frac{C - C(O_2)_2}{C - C(O_2)_1}\right) \qquad\qquad 8$$

As the diffusion rate of Oxygen is much slower in water compared to air, excess $C(H_2O)$ reduces oxygen penetration. Thus two elements: Oxygen and water vapour make up overall equation for iron oxidation as,

$$2Fe(s) + O_2(g) + H_2O(g) \longrightarrow Fe(OH)_2$$
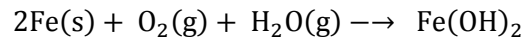
In the following section the process of iron oxidation is described.

3.4.1.1 Initial Assumptions

The following assumptions are made for the theory development:

- The layer of corrosion product is uniform along the depth of the product.
- The corrosion process, diffusion parameter values and other properties are uniform on the corroding surface.

3.4.1.2 Oxygen transport mechanism

The oxygen transport and corrosion rate is limited due to the corrosion product build-up on corroding Iron surfaces as shown in Figure 6. Figure 6 (a) represents the profile for the trend of actual Oxygen concentration $C(O_2)$, through water vapour surrounding the corroding iron and through the corrosion product. The lower part represents the current densities across various phases due to the diffusion of oxygen through the surrounding environment. However, minimum threshold concentration is required for the oxygen diffusion to take place. From Figure 7 it is evident that corrosion current density, $i(t)$ is directly related to instantaneous corrosion rate $c(t)$, and time of exposure, which in-turn directly relates to metal loss rate, $\frac{dm}{dt}$.
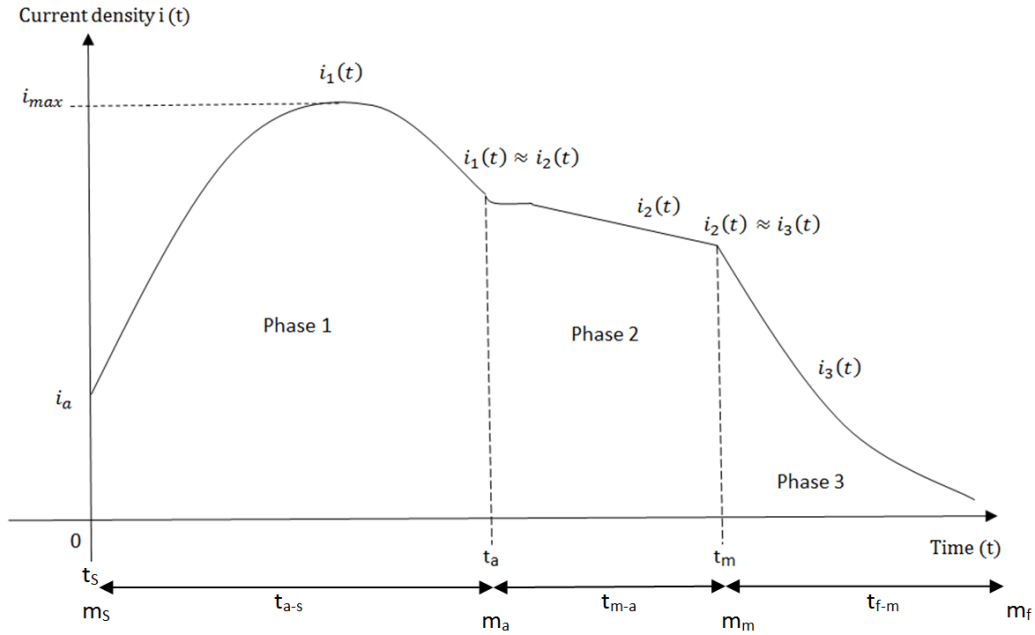
Figure: 7 Corrosion Current Density vs Time

Metal loss occurs due to the metal oxidation as a result of electrochemical reactions when oxygen transport occurs towards the corroding iron surface. Figures 6 and 7 illustrate the decreasing trends of oxygen concentration and current density with time respectively. These deceasing trends are due to two resistive layers in the path of oxygen transport. In other words oxygen transport towards the corroding iron is controlled by water vapours and the corrosion product (rust). Thus the corrosion current density at any time instance, 't' is given as;

$$i(t) = min[i_1(t), i_2(t), i_3(t)] \qquad 9$$

The point of interface of phase 1 and phase 2 is termed as t_a on the time scale. Similarly for phase 2 and phase 3 the interface point is termed as t_m. Normally the function in equation 9 will consider the value of $i_3(t)$ just after phase 3 has started, as the use of min function in equation 9 indicates that the lowest value among $i_1(t)$, $i_2(t)$ and $i_3(t)$ controls the corrosion rate .

Corrosion rate $c(t)$ can be represented by simple modified Fick's equation in which diffusion coefficient D(T), is a variable term dependent on Temperature (T). Similarly concentration C is also a variable term, dependent on ρ_w and corrosion rate is directly proportional to the corrosion current density $i(t)$.

$$c(t) \propto i(t) = \frac{D(T)\,C\,n\,F}{\delta(t)} \ln\left(\frac{C - C(O_2)_2}{C - C(O_2)_1}\right) \qquad 10$$

$$c(t) = \frac{dm}{dt} \propto i(t) = \frac{D(T)\,C\,n\,F}{\delta(t)} \ln\left(\frac{C - C(O_2)_2}{C - C(O_2)_1}\right) \qquad 11$$

n is the number of electrons participating in the oxidation of Iron, F is the Faraday's constant, D is the oxygen diffusivity through water vapours, δ is the thickness in water vapour , $\frac{dm}{dt}$ is the constant of proportionality, termed as metal loss rate.

In next sub-sections, each phase is described and expressions will be developed for t_a and t_m based on the above discussion and formulation.

3.4.1.3   Phase 1: Process Activation Phase

In this phase minimum values for both variables T and RH should be attained in order to start the process. During this phase at time t = 0, $C_B(O_2) = 0$, $D_B(T) = 0$ and the rust thickness R(t) = 0.Where $C_B(O_2)$ is the Bulk oxygen concentration in water vapour along a concentration gradient profile besides bare Iron interface and $D_B(T)$ is the diffusivity of Bulk oxygen concentration. The term $i_a(t)$ is the minimum current density that initialises just after threshold concentration is achieved at time t_a. The current density $i_a(t)$ reaches to maximum value $i_{max}(t)$ at condition $C(O_2) = C_B(O_2)$ and $D(T) = D_B(T)$. So corrosion rate and current density will be high at this point. Experimental data shows a slight decrease in the value of current density after $i_{max}(t)$ is achieved as shown in Figure 7. This decrease accounts for the oxygen to settle down after reaching maximum value. The time dependent value of current density for phase 1 is termed as $i_1(t)$. Thus the eq. for phase 1, when bulk concentration is achieved is written as,

$$c(t) = \frac{dm}{dt} = X_1 i_1(t) = \frac{D_B(T) C \, n \, F \, X_1}{\delta(t)} \ln\left(\frac{C - C_B(O_2)_2}{C - C_B(O_2)_1}\right) \qquad 12$$

Here X_1 is the constant of proportionality. It is supposed that the metal loss $m(t)$ is directly proportional to oxygen concentration gradient $\delta(t)$ through water vapour so, $m(t) \propto \delta(t)$ and $\delta(t) = m(t)A$ where **A** is the concentration gradient per unit metal loss.

When threshold condition is met, then if the distance between planes 1 and 2 is zero then $C_B(O_2)_2 = C_B(O_2)_1$ which means c(t) = 0. This shows that in order for the corrosion process to initiate after threshold, planes 1 and 2 should have gradual difference in Bulk Oxygen concentration. Eq. 12 is modified in terms of metal loss as,

$$m(t) = \sqrt{\frac{D_B(T) C \, n \, F}{A} \ln\left(\frac{C - C_B(O_2)_2}{C - C_B(O_2)_1}\right) t} \qquad 13$$

Applying boundary condition at eq.13

$$t_{a-s} = t_a - t_s = \frac{(m_a)^2 - (m_s)^2}{\frac{D_R(T) \, C \, n \, F \, X_1}{A} \ln\left(\frac{C - C_B(O_2)_2}{C - C_B(O_2)_1}\right)} \qquad (\, m_s < m < m_a \,) \qquad 14$$

$$(\, t_s \leq m \leq t_a \,)$$

At the starting time ($t_s = 0$), the metal loss m_s is also zero, thus eq. 14 can be used to find activation time t_a.

$$t_{a-s} = t_a = \frac{(m_a)^2}{\frac{D_R(T) \, C \, n \, F \, X_1}{A} \ln\left(\frac{C - C_B(O_2)_2}{C - C_B(O_2)_1}\right)} \qquad (\, m_s < m < m_a \,) \qquad 15$$

$$(\, t_s \leq m \leq t_a \,)$$

3.4.1.4   Phase 2: Process Controlling Phase

The consumption of oxygen at the Iron surface depends on the oxygen transfer from the bulk concentration to the corroding Iron surface as shown in Figure 6. As oxygen transport is the key element that controls the corrosion process, therefore phase 2 is termed as process controlling phase. The oxygen consumption, as a result of electrochemical reaction at iron surface results in the formation of corrosion product. The thickness of corrosion product is represented as R(t) in Figure 6. Initially before the formation of corrosion product **R(t) = 0**. At this point the diffusion of oxygen through water vapour starts towards iron, increasing the thickness from $0 \rightarrow R(t)$. The net concentration driving oxygen through water vapours is given as; $\ln\left(\frac{C - C_R(O_2)}{C - C_B(O_2)}\right)$. Where $C_R(O_2)$ is the effective concentration of oxygen

corresponding to plane 2 which is required to drive it through water vapour layer. High $\ln\left(\frac{C-C_R(O_2)}{C-C_B(O_2)}\right)$ value results in higher corrosion rate. The eq. for this phase is,

$$c(t) = \frac{dm}{dt} = X_2 i_2(t) = \frac{D_B(T)\, C\ n\, F X_2}{\delta(t)} \ln\left(\frac{C-C_R(O_2)}{C-C_B(O_2)}\right) \qquad \qquad 16$$

Here X_2 is the constant of proportionality. For phase 2 it is assumed that, $\delta(t) = m(t)B$ where **B** is the concentration gradient per unit metal loss. Replacing $\delta(t)$ with $m(t)B$ in eq.16 gives eq.17 in terms of metal loss $m(t)$ as,

$$m(t) = \sqrt{\frac{D_B(T)\, C\ n\, F\, X_2}{B} \ln\left(\frac{C-C_R(O_2)}{C-C_B(O_2)}\right) t} \qquad \qquad 17$$

Applying boundary condition at eq.15

$$|\, t_{m-a}| = |t_m - t_a| = \left|\frac{(m_m)^2 - (m_a)^2}{\frac{D_R(T)\, C\ n\, F X_2}{B} \ln\left(\frac{C-C_R(O_2)}{C-C_B(O_2)}\right)}\right| \qquad (\, m_m < m < m_a\,) \qquad 18$$

$$(\, t_a \leq m \leq t_m \,)$$

3.4.1.5 Phase 3: Process Subsiding Phase

As Iron corrodes further, **R(t)** becomes more and more thicker, in turn subsiding the diffusion of oxygen towards the iron, hence decreasing the current density and corrosion rate as shown in Figures 6 and 7. As thickness of the corrosion product is directly proportional to the metal loss, therefore **R(t) ∝ m(t),** which can be written as **R(t) = m(t)E**. E is the ratio of thickness of rust layer **R(t)** to the metal loss **m(t).** The resistance of the rust layer will need increased portion of oxygen concentration $C_R(O_2)$ for oxygen diffusion with increase in R(t). Thus only $C_R(O_2)$ controls the diffusion rate of oxygen as $C_m(O_2)$ is zero inside the term, $(C_R(O_2) - C_m(O_2))$ as shown in Figure 7. The eq. for this phase is,

$$c(t) = \frac{dm}{dt} = X_3 i_3(t) = \frac{D_R(T)\, (C_R(O_2) - C_m(O_2))\, n\, F\, X_3}{R(t)} \qquad \qquad 19$$

X_3 is the constant of proportionality and D_R is the diffusion of oxygen through corrosion product, replacing **R(t)** with **m(t)E** eq.19 yields

$$m(t) = \sqrt{\frac{D_R(T)\, C_R(O_2)\ n\, F\, X_3}{E} t} \qquad \qquad 20$$

As **R(t)** increases $C_R(O_2)$ also increases. The bulk Oxygen concentration $C_B(O_2)$ does not affect Oxygen diffusion through the rust layer. Just after start of phase 3 at point t_m the current density i_2 equals i_3. Using eq.18 to calculate t_m and applying boundary condition on eq.20.

$$t_{f-m} = t_f - t_m = \frac{(m_f)^2 - (m_m)^2}{\frac{D_R(T)\, C_R(O_2)\ n\, F\, X_3}{E}} \qquad (\, m_f < m < m_m\,)$$

$$(\, t_m \leq t \leq t_f\,) \qquad 21$$

m_m and m_f represent initial and final metal-loss value respectively while t_{f-m} represent the process time spent during phase 3 and t_f is the final time at which the process ceases.

Eq. 9 can be modified in terms of corrosion current densities calculated for all phases,

$$i(t) = \min\left[\frac{D_B(T)C\, n\, F}{\delta(t)} \ln\left(\frac{C-C_B(O_2)_2}{C-C_B(O_2)_1}\right),\quad \frac{D_B(T)\, C\ n\, F}{\delta(t)} \ln\left(\frac{C-C_R(O_2)}{C-C_B(O_2)}\right),\quad \frac{D_R(T)\, (C_R(O_2)\, n\, F}{R(t)}\right] \qquad 22$$

Equation 12 shows the relationship of metal loss rate $\frac{dm}{dt}$ during phase 1 considering the condition, relating time of exposure as; $t < t_a$. In this descriptive model, a linear increase in oxygen concentration is assumed, before the required threshold concentration is achieved based on limited experimental data available from already available reported research work. Figures 6 and 7 indicate the decay in corrosion rate right after the initiation of phase 2 with the gradual development of passive corrosion layer on metal surface. The time of exposure in phase 2 is related as, $t_a \leq t \leq t_m$. It is observed that the metal loss rate $\frac{dm}{dt}$ in phase 2 is directly dependent on gradient of oxygen transport indicated as $\ln\left(\frac{C-C_R(O_2)}{C-C_B(O_2)}\right)$. Of course, higher bulk concentration of oxygen, $C_B(O_2)$ account for higher corrosion rate and higher $C_R(O_2)$ account for gradual decrease in gradient value due to the corrosion product formation on metal surface. The gradual fall in the current density comes to end, when $t = t_m$ after which corrosion process enters into phase 3 showing exponential decay in the current density as shown in Figure 7. The time of exposure in phase 3, $t_m \leq t \leq t_f$ depends on t_f when oxygen transport completely becomes ignorable. In this phase, oxygen transport only depends on $C_R(O_2)$ as the term $C_m(O_2) \approx 0$ in gradient factor $(C_R(O_2) - C_m(O_2)$.

The metal loss equations 13, 17 and 20, derived are closely in relation with the experimental results. These are useful for the understanding of basic studies regarding the oxygen transport and corrosion product formation for conditions where coatings have failed but no surface or atmospheric pollutants. Equations 12, 16 and 19 clearly indicate that the corrosion rate depends on the concentration of oxygen in the environment. When RH is sufficient in the environment with sufficient temperature, only then the oxygen transport could take place as justified in ACCM. Both parameters; T and RH are important but to avoid corrosion product formation, RH should be kept within the Safe Zone shown in Table 6. During phase 2, the concentration gradient equation, $\ln\left(\frac{C-C_R(O_2)}{C-C_B(O_2)}\right)$ gives a direct relationship with metal loss rate. So, if $\ln\left(\frac{C-C_R(O_2)}{C-C_B(O_2)}\right) \approx 0$ because $C_B(O_2) = C_R(O_2)$, this condition indicates that the RH in the environment is under controlled condition and $c(t) = \frac{dm}{dt} = 0$. On the other hand if $C_B(O_2) > C_R(O_2)$, then the environment can be categorised as under critical condition and therefore $c(t) = \frac{dm}{dt} > 0$.

Table 6 Various Zones for Corrosion Depending upon Concentration Gradient Profile

Environmental Zones	ACCM Conditions	Real Conditions	Corrosion rate, $c(t)$
Safe Zone	$C_B(O_2) < C_R(O_2)$	0 % – 45 % RH	$c(t) = \dfrac{dm}{dt} = 0$
Mild Zone	$C_B(O_2) = C_R(O_2)$	45 % – 55 % RH	
Critical Zone	$C_B(O_2) > C_R(O_2)$	> 55% RH	$c(t) = \dfrac{dm}{dt} > 0$

4 Conclusion

Surface corrosion mechanisms, propagation to sub-surface and contaminants have been identified within the sample collected from the large military vehicle. During simulated environmental tests, even at the optimum environmental conditions some degree of corrosion accumulation was recorded. The multiple phase ACCM model was used to monitor the corrosion rate for this particular large vehicle. This model can be used to identify the temperature-relative humidity relationship for minimum metal loss. ACCM can also be deployed to predict the time gap between corrosion initiation and termination, provided to use forecasting for final time value, t_f in eq. 21. This can be done using forecasting tools.

During this research it was found that the existing environmental conditions of the sheltered facility for the large military vehicles are not suitable for the structural health of these vehicles. It is important to achieve the optimum temperature and humidity levels to minimise the aging process of these vehicle through corrosion. This method of controlled environment is non-invasive and is sustainable. Vehicle's surfaces which display failures in paints/coatings require enhanced protection. In addition conditioning of surfaces through anti-corrosive agents is also very important as contaminants play vital role as catalyst in corrosion initiation and propagation.

Acknowledgements

References

[1] B.K. Yueping Wang, Review of Corrosion Control Programs and Research Activities for army Vehicles Defence Research and Development Canada, Defence R&D Canada- Atlantic, 2006, 1- 35.

[2] DoD. USA, Corrosion Prevention and Mitigation Strategic Plan, 2011, 1-136.

[3] A. Saeed, Z. A. Khan, M. Hadfield, S. Davies, Material characterization and real-time wear evaluation of pistons and cylinder liners of the tiger 131 military tank, Tribology Transactions, 56 (2013) 637-644.

[4] A. Saeed, Z.A. Khan, E. Montgomery, Corrosion Damage Analysis and material Characterization of Sherman and Centaur - The Historic Military Tanks, Materials Performance and Characterization, 2 (2013.) 30-44.

[5] K. Wilton-Smith, Z. A. Khan, A. Saeed, M. Hadfield, Accelerated corrosion tests of waste-gated turbocharger's adjustable and fixed end links, presneted in International Conference on High Performance and Optimum Design of Structures and Materials, WIT Press, 9 - 11 June, 2014 Ostend, Belgium, 501-508.

[6] A. Saeed, Z.A. Khan, N. Garland, R. Smith, Material characterisation to understand various modes of corrosion failures in large military vehicles of historical importance, presneted in Fifth International Conference on Computational Methods and Experiments in Materials Characterisation, 13 - 15 June 2011, WITpress, Kos, Greece, 95-106.

[7] A. Saeed, Z. Khan, M. Clark, N. Nel, R. Smith, Non-destructive material characterisation and material loss evaluation in large historic military vehicles, Insight: Non-Destructive Testing and Condition Monitoring, 53 (2011) 382-386.

[8] Z. A. Khan, M. Grover, M.H. Nazir, The Implications of Wet and Dry Turning on the Surface Quality of EN8 Steel, Transactions on Engineering Technologies, Springer, 2015, pp. 413-423.

[9] Z. A. Khan, P. Pashaei, R.S. Bajwa, M.H. Nazir, M. Camak, Fabrication and characterisation of electrodeposited and magnetron sputtered thin films, International Journal of Computational Methods & Experimental Measurements, 3 (2015) 165-174.

[10] M. Nazir, Z.A. Khan, K. Stokes, A unified mathematical modelling and simulation for cathodic blistering mechanism incorporating diffusion and fracture mechanics concepts, Journal of Adhesion Science and Technology, 29 (2015) 1200-1228.

[11] M. Nazir, Z.A. Khan, K. Stokes, Optimisation of interface roughness and coating thickness to maximise coating–substrate adhesion–a failure prediction and reliability assessment modelling, Journal of Adhesion Science and Technology, 29 (2015) 1415-1445.

[12] M.H. Nazir, Z. Khan, K. Stokes, Modelling of metal-coating delamination incorporating variable environmental parameters, Journal of Adhesion Science and Technology, 29 (2014) 392-423.

[13] M.H. Nazir, Z.A. Khan, K. Stokes, Maximising the interfacial toughness of thin coatings and substrate through optimisation of defined parameters, International Journal of Computational Methods & Experimental Measurements, 3 (2015) 316-328.

[14] M.H. Nazir, Z.A. Khan, K. Stokes, A holistic mathematical modelling and simulation for cathodic delamination mechanism – a novel and an efficient approach, Journal of Adhesion Science and Technology, (2015) 1-39.

[15] M. H. Nazir, Z. A. Khan, A. Saeed, K. Stokes, Modelling the Effect of Residual and Diffusion induced Stresses on Corrosion at the Interface of Coating and Substrate, CORROSION, 72(4), (2016) 500-517.

[16] M. H. Nazir, Z. A. Khan, A. Saeed, K. Stokes, A model for cathodic blister growth in coating degradation using mesomechanics approach Materials and Corrosion, (2015).

[17] A. Saeed, Sustainable methodology of conserving historic military vehicles, Bournemouth University, Thesis (2013) 60-112.

[18] J. Porges, F. Porges, Handbook of heating, ventilating and air conditioning : ready-reference tables and data, 7th ed. / revised by F. Porges. ed., Newnes-Butterworths, London, 1976.

[19] ISO. Standards, Corrosion of metals and alloys Corrosivity of atmospheres Classification, determination and estimation, International Organization for Standards, Geneve, Switzerland, (1992) 1-15.

[20] P.A. Schweitzer, Fundamentals of corrosion : mechanisms, causes, and preventative methods, CRC, Boca Raton, Fla., 2010.

[21] A.K. Neufeld, I.S. Cole, A.M. Bond, S.A. Furman, The initiation mechanism of corrosion of zinc by sodium chloride particle deposition, Corrosion Science, 44 (2002) 555-572.

[22] H.J. Grabke, E. Reese, M. Spiegel, The effects of chlorides, hydrogen chloride, and sulfur dioxide in the oxidation of steels below deposits, Corrosion Science, 37 (1995) 1023-1043.

[23] D. Maiti, P. Sujatha Devi, Selective formation of iron oxide and oxyhydroxide nanoparticles at room temperature: Critical role of concentration of ferric nitrate, Materials Chemistry and Physics, 154 (2015) 144-151.

[24] Y. Ma, Y. Li, F. Wang, The effect of β-FeOOH on the corrosion behavior of low carbon steel exposed in tropic marine environment, Materials Chemistry and Physics, 112 (2008) 844-852.

[25] B.P. Haigh, Part II: slag inclusions, welding and soldering. Slag inclusions in relation to fatigue, Transactions of the Faraday Society, 20 (1924).

[26] H.H. Kart, M. Uludogan, T. Cagin, DFT studies of sulfur induced stress corrosion cracking in nickel, Computational Materials Science, 44 (2009) 1236-1242.

[27] M. Yamaguchi, M. Shiga, H. Kaburaki, Grain boundary decohesion by impurity segregation in a nickel-sulfur system, Science, 307 (2005) 393-397.

[28] R. Kiessling, N. Lange, Non-metallic inclusions in steel, 2nd ed. ed., Metals Society, London, 1978.

[29] D.E. Williams, M.R. Kilburn, J. Cliff, G.I.N. Waterhouse, Composition changes around sulphide inclusions in stainless steels, and implications for the initiation of pitting corrosion, Corrosion Science, 52 (2010) 3702-3716.

[30] G. Wranglen, Pitting and sulphide inclusions in steel, Corrosion Science, 14 (1974) 331-349.

[31] T.L. Anderson, Fracture mechanics : fundamentals and applications, 3rd ed. ed., Taylor & Francis, Boca Raton, Fla. ; London, 2005.

[32] N.K. Das, I. Tirtom, T. Shoji, A multiscale modelling study of Ni–Cr crack tip initial stage oxidation at different stress intensities, Materials Chemistry and Physics, 122 (2010) 336-342.

[33] J. Tidblad, A.A. Mikhailov, V. Kucera, Model for the prediction of the time of wetness from average annual data on relative air humidity and air temperature, Protection of Metals, 36 (2000) 533-540.

[34] T.G. C. Leygraf, Atmospheric Corrosion, Wiley-Interscience, John Wiley and Sons, 2000.

[35] L. S. Lyon, Corrosion of Carbon and Low Alloy Steels, Shreir's Corrosion, Elsevier, Oxford, 2010, pp. 1693-1736.

[36] F. Corvo, T. Pérez, Y. Martin, J. Reyes, L.R. Dzib, J. González-Sánchez, A. Castañeda, Time of wetness in tropical climate: Considerations on the estimation of TOW according to ISO 9223 standard, Corrosion Science, 50 (2008) 206-219.

[37] P. Montoya, I. Díaz, N. Granizo, D. de la Fuente, M. Morcillo, An study on accelerated corrosion testing of weathering steel, Materials Chemistry and Physics, 142 (2013) 220-228.